ACS APPLIED MATERIALS & INTERFACES

Research Article

www.acsami.org

Correlating the Local Defect-Level Density with the Macroscopic Composition and Energetics of Chalcopyrite Thin-Film Surfaces

Sebastian Bröker,[†,‡,§] Dennis Kück,[†,‡,§] Alexander Timmer,[†,‡,§] Iver Lauermann,[⊥] Bünyamin Ümsür,[⊥] Dieter Greiner,[⊥] Christian A. Kaufmann,[⊥] and Harry Mönig*[,†,‡]

[†]Physikalisches Institut, Westfälische Wilhelms-Universität Münster, Wilhelm-Klemm-Strasse 10, 48149 Münster, Germany

[‡]Center for Nanotechnology (CeNTech), Heisenbergstrasse 11, 48149 Münster, Germany

[⊥]Helmholtz-Zentrum Berlin für Materialien und Energie, Hahn-Meitner-Platz 1, 14109 Berlin, Germany

Supporting Information

ABSTRACT: The unusual defect chemistry of polycrystalline Cu(In,Ga)Se_2 (CIGSe) thin films is a main issue for a profound understanding of recombination losses in chalcopyrite thin-film solar cells. Especially, impurity-driven passivation of electronic levels due to point defects segregating at the surface and at grain boundaries is extensively debated. By combining current imaging tunneling spectroscopy with photoelectron spectroscopy, the local defect-level density and unusual optoelectronic grain-boundary properties of this material are correlated with the macroscopic energy levels and surface composition. Vacuum annealing of different CIGSe materials provides evidence that Na diffusion from the glass substrate does not affect the surface defect passivation or grain-boundary properties of standard Cu-poor materials. Furthermore, we find no major impact on the observed thermally activated dipole compensation or the accompanying change in surface band bending (up to 0.6 eV) due to Na. In contrast, Cu-rich CIGSe shows an opposing surface defect chemistry with only minor heat-induced band bending. Our results lead to a comprehensive picture, where the highly desirable type inversion at the p/n interface in standard chalcopyrite thin-film solar cells is dominated by band bending within the CIGSe absorber rather than the result of Na impurities or an n-type defect phase segregating at the interface. This is in accordance with recent studies suggesting a surface reconstruction as the origin for Cu depletion and band-gap widening at the surface of chalcopyrite thin films.

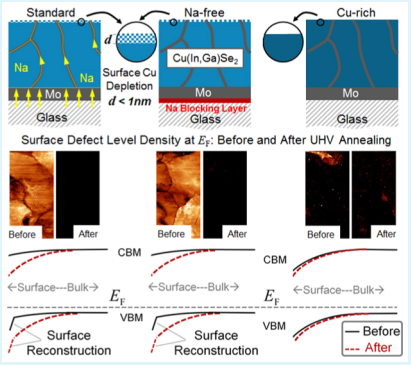

KEYWORDS: *chalcopyrite thin films, solar cells, surface defects, scanning tunneling spectroscopy, photoelectron spectroscopy*

INTRODUCTION

In the last 2 years, chalcopyrite thin-film solar cells based on Cu(In,Ga)Se_2 (CIGSe) as absorber material have shown record conversion efficiencies of up to 21.7%, most remarkably exceeding the performance of conventional devices based on polycrystalline silicon.[1−3] The standard device structure and a corresponding energy-level diagram of the heterojunction is sketched in Figure 1. Excellent absorption properties of the CIGSe material, the superior long-term stability, and the possibility of applying large-area thin-film deposition techniques for module production lead to an attractive balance of cost and efficiency for this technology. Further efficiency improvements above 25% seem to be possible via improvements of the open-circuit voltage and fill factor.[4] However, this requires a profound understanding of recombination mechanisms, which are strongly related to the complex defect chemistry of the chalcopyrite material. In fact, these devices are by far not as well understood as conventional silicon solar cells, which is mainly due to the low formation energies for point defects and the related high tolerance for off-stoichiometry.[5−7] Understanding the factors that determine the anomalous optoelectronic grain-bounary properties and the defect-level density at the CIGSe/CdS heterojunction is probably the key for further efficiency gains. In particular, with a grain size of about 1−2 μm, chalcopyrite thin films exhibit an extremely high density of grain boundaries, which is orders of magnitude higher compared to crystalline silicon-based devices. Considering grain-boundary recombination, a major loss mechanism for the device performance, the high efficiency of chalcopyrite-based solar cells is astonishing. Therefore, chalcopyrite grain-boundary properties have been the subject of intense controversial discussion in the literature for many years.[8−14]

Concerning the defect chemistry at the CIGSe/CdS interface, a Cu-deficient layer, which is observed at the free CIGSe surface, is believed to largely determine the electronic properties and recombination losses.[15] The pronounced surface Cu depletion with respect to the bulk of slightly Cu-poor grown material lowers the valence-band maximum (VBM) at the surface/interface, leading to a band-gap widening of about 200−300 meV relative to the (integral) bulk band gap (1.2 eV;

Received: April 15, 2015
Accepted: May 26, 2015
Published: May 26, 2015

DOI: 10.1021/acsami.5b03260
ACS Appl. Mater. Interfaces 2015, 7, 13062−13072

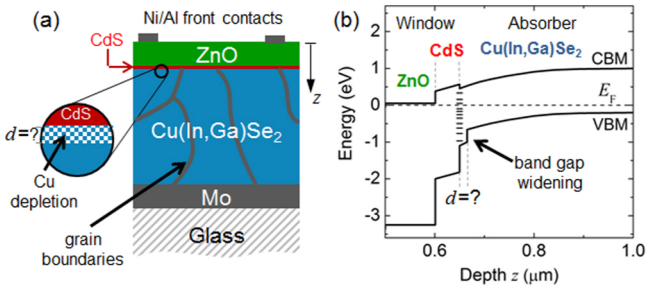

Figure 1. (a) Schematic diagram of the standard device structure of a chalcopyrite thin-film solar cell. The 2 μm CIGSe absorber is grown on a 1 μm Mo back-contact. The window layer consists of 0.5 μm ZnO and a 50 nm CdS buffer layer. The CIGSe side of the absorber/window interface is Cu-depleted with respect to the bulk composition. (b) Corresponding energy-level diagram in the range of the heterojunction (redrawn from work by Klenk and Lux-Steiner).[25] The Cu depletion leads to a lowering of the VBM. CBM: conduction-band minimum. VBM: valence-band maximum.

Figure 1b).[16,17] Furthermore, the surface Cu depletion is believed to be closely related to a type inversion at the interface and free surface.[15] However, its structural properties and, in particular, the extension in depth d of the absorber are the subject of an ongoing debate. As shown in the energy-level diagram in Figure 1b, the importance of this topic is based on the fact that this thickness strongly affects the barrier for the thermionic contribution to interface recombination currents. A thickness d restricted to only a few atomic layers would strongly increase tunneling contributions, whereas a spatially more extended Cu-depleted region would prevent tunneling as the source for interface recombination.

As an explanation of the surface Cu depletion, there are three main models under discussion: (i) a defect phase with bulklike properties and n-type conductivity segregating at the surface,[15,18] (ii) electromigration of Cu atoms in the surface field of the space charge region into the bulk,[19−21] and (iii) a surface reconstruction model, where under Cu-poor conditions only the top few atomic layers are subjected to elemental rearrangements involving a high density of Cu vacancies and (In,Ga)-on-Cu antisite defects.[6,22−24]

Regarding both the CIGSe/CdS interface and grain boundaries, the crucial question becomes whether passivation mechanisms in the material are intrinsic or due to the presence of impurities like O, elements from the window layer (Cd, Zn, or S), or Na diffusion from the glass substrate.[8,10−12,26−30] In fact, the introduction of alkali metal containing soda lime glass as substrates for the devices led to significant efficiency improvements in the early 1990s. Meanwhile, Na is known to diffuse during film growth into the chalcopyrite film, where it accumulates at grain boundaries and at the surface/interface.[31,32] Moreover, the development of additional alkali-metal postdeposition treatments has led to the very recent efficiency gains.[1−3] Both the beneficial effects of Na diffusion from the glass substrate and the postdeposition treatments are barely understood.

Usually, defect spectroscopy of semiconductors is performed with integral methods, which only allow indirect conclusions about the localized defect chemical properties at interfaces. Therefore, in the present work, we investigate the local electronic defect-level density of different CIGSe samples by scanning tunneling spectroscopy (STS), which is a well-established tool in surface science to experimentally assess the density of states of a sample on a nanometer scale. In STS experiments, the tunneling current between a sharp metallic tip and the sample surface is analyzed as a function of the applied bias voltage $I(U)$. The differential conductivity can be approximated as proportional to the density of states $dI/dU \propto$ DOS. By controlling the bias voltage polarity in the measurements, occupied and unoccupied states can be probed in an energy range of a few electronvolts around E_F. When the $I(U)$ spectra are recorded on a fine equally spaced grid [current imaging tunneling spectroscopy (CITS)], dI/dU maps are obtained, which are interpreted in terms of the local electronic defect-level density at different energies eU. Furthermore, locally resolved STS allows one to study the lateral band-bending effects at grain boundaries.[33,34] Combining dI/dU mapping with UV, soft, and hard X-ray photoelectron spectroscopy (UPS/XPS/HAX-PES) allows one to correlate the local defect-level density with the integral energy-level alignment, dipole formation, and chemical composition at the surface of the investigated CIGSe samples. Note that, in general, these techniques can be classified as surface-sensitive. Nevertheless, they comprise slightly different information depths: synchrotron excited HAX-PES allows to control the information depth via the tunable excitation energy in a range of 6−25 nm; XPS experiments usually have an information depth of 3−5 nm; UPS experiments can be estimated to probe about 1 nm; in STS, the tunneling current is governed by the outermost orbitals, leading to an information depth even below 1 nm.

In our study, we compare standard Cu-poor CIGSe, grown by elemental coevaporation, with and without a Na diffusion barrier at the Mo back-contact. In addition, Cu-rich samples, where the growth process was terminated during the Cu-rich growth stage, are investigated to assess the effect of the integral Cu content on the defect chemistry and electronic properties at the surface and grain boundaries. In the following, these samples are referred to as Na-free, standard, and Cu-rich CIGSe, respectively.

Unexpectedly, our results show that the presence of Na can be excluded as the origin for passivation and lateral band bending at grain boundaries of standard absorber layers. Furthermore, we provide experimental evidence that surfaces of slightly Cu-poor chalcopyrite thin films can intrinsically passivate electronic surface defect levels and compensate surface dipoles without the presence of impurities like alkali metals, O, or elements from the window layer. Both sample materials with and without a Na diffusion barrier show a pronounced increasing surface downward band bending of up to 600 meV induced by heat treatment in ultrahigh vacuum (UHV). This is in contrast to the Cu-rich material, which after removal of secondary phases from the surface shows hardly any change in the surface band alignment. These findings show that the type inversion at the surface of standard chalcopyrite materials is dominated by band bending rather than the segregation of a bulklike defect compound with n-type conductivity at the surface. The absence of any significant lateral and vertical band-bending effects in the case of the Cu-rich material suggests that, in the case of standard Cu-poor grown CIGSe, Cu vacancies and (In,Ga)-on-Cu antisite defects at the surface or grain boundaries are responsible for an accumulation of positive charges inducing the lateral and vertical band bending in this case.

The HAX-PES experiments for standard CIGSe samples provide evidence that, after oxide removal and subsequent

DOI: 10.1021/acsami.5b03260
ACS Appl. Mater. Interfaces 2015, 7, 13062−13072

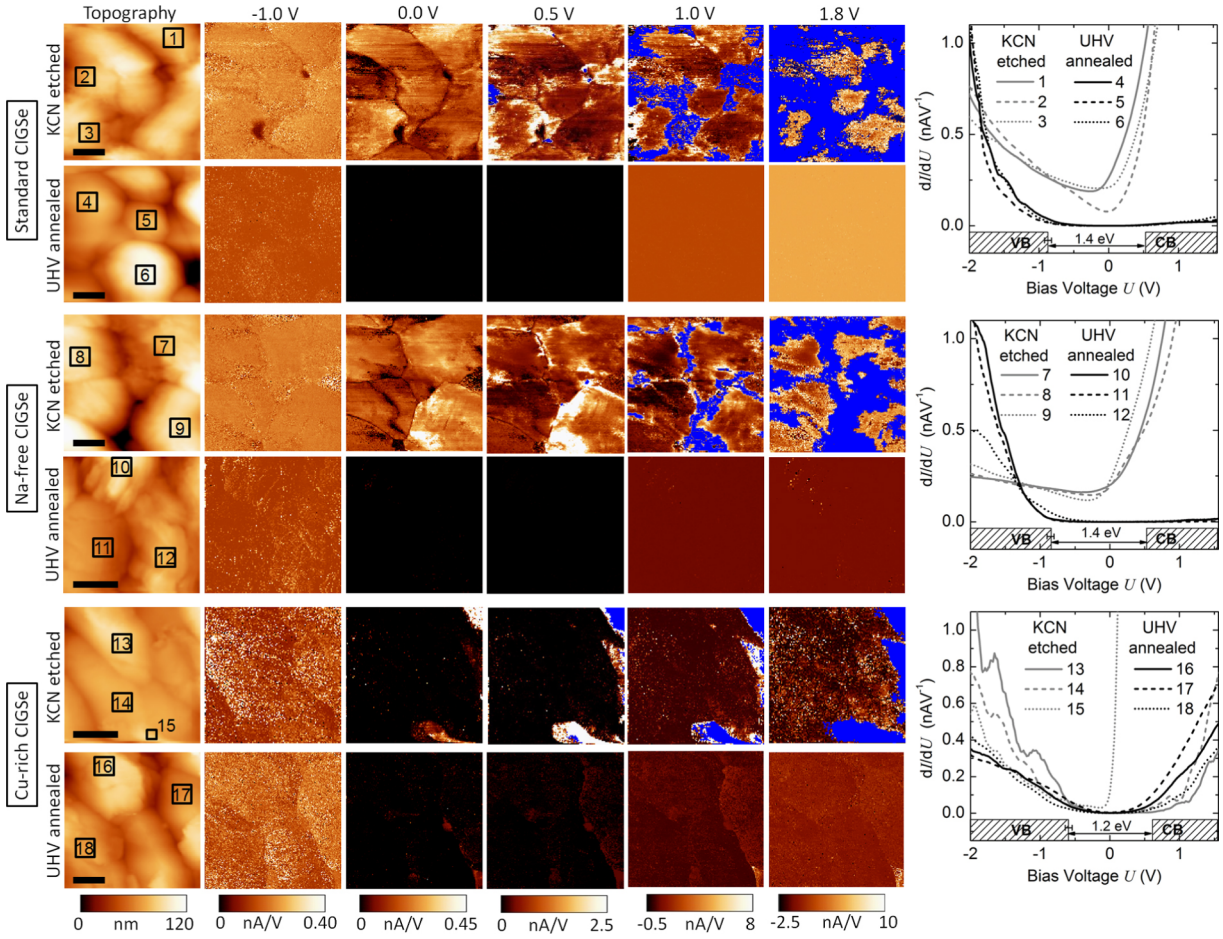

Figure 2. dI/dU maps at various bias voltages for standard, Na-free, and Cu-rich grown CIGSe before and after UHV heat treatment at 280 °C. The contrast color scales at the bottom are the same for all images in one column. The blue areas in the dI/dU maps at $U \geq 0.5$ V indicate sites where the current limit of the measurement (5 nA) is exceeded. The diagrams on the very right show spectra that are averaged from the areas surrounded by the black rectangles in the topography images. On the bias voltage axis, the corresponding energy ranges of the valence and conduction bands (VB and CB) are indicated. Thereby, the VBM is in accordance with photoelectron spectroscopy measurements for the state after UHV annealing in each case. Complete data sets are provided as dI/dU movies (see the SI). The image size is indicated by a 400 nm scale bar in the lower left of the topography images. Set-point values (U; I) in the different data sets are as follows (from the top to bottom): (−2.0 V; 0.70 nA), (−2.0 V; 0.40 nA), (−2.0 V; 0.40 nA), (−2.3 V; 0.30 nA), (−2.3 V; 0.55 nA), and (−2.3 V; 0.55 nA).

UHV heat treatment, the resulting surface type inversion goes along with a surface Cu depletion extending only a few atomic layers into the bulk of the absorber. At the same time, compositional analysis by XPS shows only a negligible correlation of the surface Cu content with the degree of surface band bending, suggesting only minor effects due to electromigration as the driving force for the surface Cu depletion. However, our findings are in agreement with the theoretical model proposing a defect-induced surface reconstruction, where recent theoretical advances demonstrated its capability to provide an explanation not only for the surface Cu depletion and dipole compensation but also for the surface band-gap widening of standard chalcopyrite absorbers.[6]

RESULTS

The polycrystalline CIGSe thin films were grown by a multistage coevaporation process with an intermediate Cu-rich growth phase on Mo-coated float glass substrates.[35] The integral Ga content of all samples was [Ga]/([In] + [Ga]) ≈ 0.3. CIGSe thin films were grown on two different types of substrates under standard conditions within the same process, resulting in a slightly Cu-poor integral composition of about [Cu]/([In] + [Ga]) = 0.78. To prevent Na diffusion from the glass substrate into the chalcopyrite film for one of the samples, a commercial Mo-coated substrate with an integrated Na diffusion barrier (Saint Gobain, Mo-SP++) was used alongside a Mo-coated standard float glass substrate. A third sample was grown in a process that was terminated after the Cu-rich growth stage, resulting in an integral composition of [Cu]/([In] + [Ga]) = 1.05. It is well-known that at this growth stage the Cu excess leads to the segregation of $Cu_{2-x}Se$ phases at the surface.[15] These copper selenides can easily be removed by an etching treatment in a wet chemical KCN solution.[36] After KCN etching, we found that the integral Cu content had reduced to [Cu]/([In] + [Ga]) = 0.93, which can be attributed to removal of the $Cu_{2-x}Se$ phases. The presence prior to and removal of copper selenides after KCN etching was verified by scanning electron microscopy (SEM; Figure S1 in the Supporting Information, SI). Although this sample state shows a slight Cu deficiency, in the following we label it as "Cu-rich sample", referring to its growth under Cu-rich conditions. Generally, exposing chalcopyrite surfaces to such a KCN treatment removes oxides and surface contaminants. Thereby, it is pointed out that a KCN treatment of (standard)

DOI: 10.1021/acsami.5b03260
ACS Appl. Mater. Interfaces 2015, 7, 13062−13072

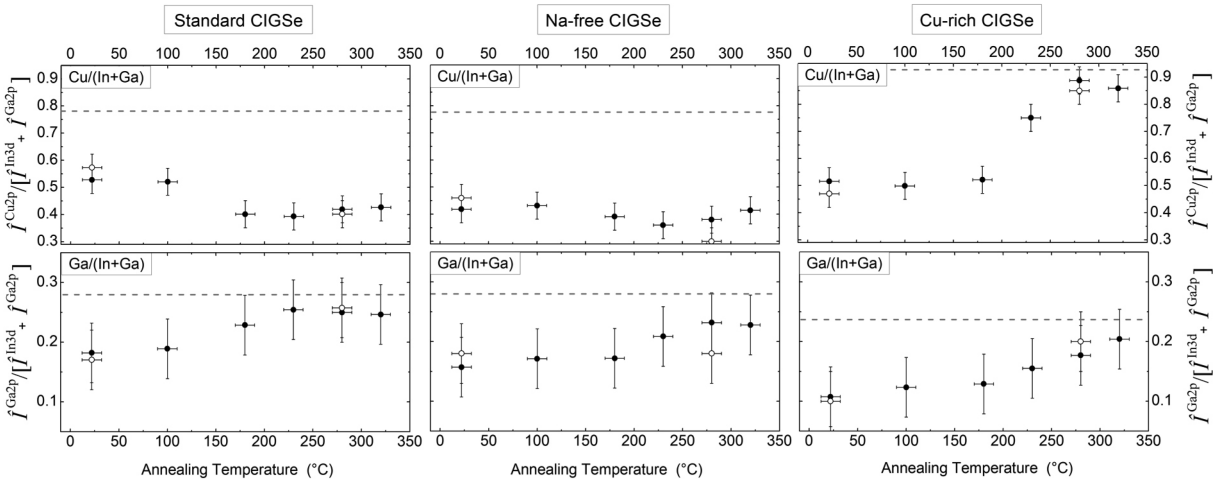

Figure 3. Relative corrected XPS intensities for Cu $2p_{3/2}$, In $3d_{5/2}$, and Ga $2p_{3/2}$. The filled circles are data points that were recorded after consecutively heating the samples to various temperatures in UHV. The open circles show data of additional experiments where a single heating step to 280 °C was applied. The data reflect changes in the relative surface composition due to the heat treatment. To compare these results with the integral composition of the samples, the horizontal dashed lines show the corresponding values as measured by X-ray fluorescence analysis.

Cu-poor grown absorber films does not alter the conversion efficiency of the finalized solar cells, but rather it preserves the surface Cu depletion and allows one to recover the photovoltaic properties of aged chalcopyrite absorbers.[24,37,38] To obtain defined and comparable surface conditions prior to our measurements, corresponding samples were etched in an aqueous KCN solution (5%) for 3 min (unless otherwise stated). After etching and subsequent rinsing in purified water, the samples were, without further air exposure, immediately transferred via an inert-gas glovebox into the STM or XPS/UPS UHV systems. In the case of the HAX-PES experiments, an air exposure of the samples during transfer into UHV of less than 30 s could not be avoided.

Figure 2 shows dI/dU maps at various bias voltages for standard, Na-free, and Cu-rich grown CIGSe. The data are presented for both the states after KCN etching and after a subsequent heat treatment at 280 °C in UHV for 30 min. As will be shown later, at this temperature Na diffusion from the glass substrate to the surface is activated. On the very right of Figure 2, the corresponding dI/dU(U) spectra are shown from the centers of three different grains, where the spectra are averaged over the rectangular areas indicated in the corresponding topography images for each data set. First, it is noted that the data for standard and Na-free CIGSe show very similar signatures. After KCN etching, both materials show a metallic dI/dU characteristic with a high density of defect levels in the energy range of the band gap. Only very few grains show a slightly reduced differential conductivity around E_F (U = 0 V), as for example, grain 2. We rarely find such partly passivated grains on standard CIGSe surfaces. An assessment of available data sets allowed to estimate that about 5−10% of the surface area shows such a reduced defect density on whole grains, which is probably related to a particular grain orientation.

At grain boundaries, the dI/dU maps at U = 0 V of the KCN-etched state for the standard and Na-free samples in both cases show a reduced dI/dU contrast. As previously reported for as-grown and KCN-etched standard CIGSe films, this can be attributed to a reduced density of (deep) defect levels close to E_F at grain boundaries.[12,39] In addition to this grain-boundary passivation both studies reported a distinct downward band bending toward the grain boundaries. Interestingly, an analysis of the CITS data sets of the standard and Na-free samples reveals a comparable lateral downward band bending toward the grain boundaries. This can be estimated by extracting single dI/dU spectra from different distances of various grain boundaries (see Figures S2 and S3 in the SI) showing distinct shifts in the spectra, which leads to pronounced gradual characteristics in the dI/dU movies at positive bias voltages (movies provided as SI). Note that directly on grain boundaries the band-bending effect and changes in the density of states are present at the same time. Therefore, in Figures S2 and S3 in the SI, we discern these two effects.

After UHV annealing of the standard and Na-free samples, the surface defect levels are largely passivated for both with only minor lateral inhomogeneities from grain to grain or at grain boundaries. The corresponding STS spectra (4 to 6 and 10 to 12 in Figure 2) can be compared with the assumed energy-level alignment at the surface, which is indicated at the bias voltage axis. Here, the VBM was determined by photoelectron spectroscopy for the sample state after UHV annealing (Figure S5 in the SI). The alignment of the CBM is estimated by assuming an enlarged surface band gap of 1.4 eV, which is in agreement with reported values in the literature.[6,16,17,30,39] Because the density of states in the CB is about an order of magnitude lower compared to the VB, the STS data do not allow to directly determine the band gap. However, the STS spectra show a reasonable agreement with the indicated band-gap region.

While the STS data of the standard and Na-free absorbers show very similar STS characteristics, the Cu-rich grown material shows significant differences. After KCN etching, the surface appears to be widely passivated, where we do not observe any significant band-bending effects (see Figure S4 and the corresponding dI/dU movie in the SI). However, there are small areas with an extremely high differential conductivity at positive bias voltages (see, e.g., averaged spectra 15). Within these areas, band-bending effects are observed, pointing to upward as well as downward band bending toward grain boundaries (Figure S4 in the SI). From the analysis of several data sets, we estimate that about 5−10% of the surface shows such high conductance. Disregarding these high conductance areas, the spectra show semiconducting characteristics (spectra

DOI: 10.1021/acsami.5b03260
ACS Appl. Mater. Interfaces 2015, 7, 13062−13072

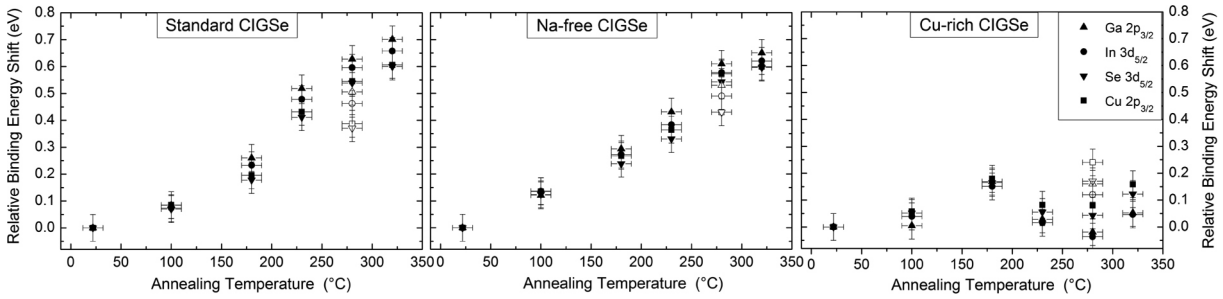

Figure 4. XPS core-level binding energy shifts determined after the samples were heated consecutively to various temperatures in UHV. All data points are normalized to the state without any heat treatment. The significant collective peak shifts to higher binding energies observed for the standard and Na-free samples reflect a pronounced increasing downward band bending with increasing temperature. In contrast, the Cu-rich sample shows only minor band-bending effects. The open circles in the diagrams show data from additional experiments where only a single heating step to 280 °C was performed.

13 and 14 in Figure 2). After UHV annealing, no significant changes of the band gap or its alignment with respect to E_F are observed. Only the mentioned areas with extremely high differential conductivity seem to be absent or significantly reduced in dI/dU at $U > 0$ V. In the same way as for the other two samples, the energy-level alignment for the case after UHV annealing is shown at the bias voltage axis. Hereby, we considered a surface band gap that is 0.2 eV smaller than that in the case of the Cu-poor grown material.[6]

To elucidate compositional and electronic changes of the three different materials due to the UHV heat treatment, XPS experiments were performed. For each sample, first the KCN-etched state was measured. Then it was subsequently heated to various temperatures (each for 30 min) in a range of 100 °C ≤ T ≤ 320 °C in UHV. To analyze potential heat-induced compositional changes, we quantitatively evaluated XPS core-level intensities $I^{\psi_{n,l}}$, determined by calculating the peak areas. These experimental intensities are then corrected by the corresponding sensitivity factors for our experimental setup. In the following, the resulting corrected intensities are termed $\hat{I}^{\psi_{n,l}}$ for the core level $\psi_{n,l}$. Note that, assuming the concentration of an element k to be constant in depth, the corrected intensities are a direct measure for the concentration $\hat{I}_k^{\psi_{n,l}} = C_k$. However, as discussed below, the investigated CIGSe materials show concentration changes within the XPS information depth. Therefore, we analyze our data strictly in terms of the corrected intensities.

Figure 3 displays the $\hat{I}^{Cu\ 2p}/(\hat{I}^{In\ 3d} + \hat{I}^{Ga\ 2p})$ and $\hat{I}^{Ga\ 2p}/(\hat{I}^{In\ 3d} + \hat{I}^{Ga\ 2p})$ relative corrected intensities for the Cu $2p_{3/2}$, In $3d_{5/2}$, and Ga $2p_{3/2}$ core-level lines. After KCN etching, all three samples show values pointing to a Cu-depleted surface stoichiometry with respect to the bulk composition (top row in Figure 3). After the annealing step to 170 °C, the standard CIGSe sample shows a slight steplike decrease, which points to a further reduction of the relative surface Cu content. In contrast, the Na-free sample shows overall a surface stoichiometry close to the values of the standard sample after annealing to $T \geq 170$ °C with only minor changes of the values with the annealing temperature. The distinct and reproducible heat-induced reduction of the relative Cu content in the case of the standard material is attributed to the different degree of surface oxidation for the standard and Na-free material in the as-grown state. Both sample materials have experienced a similar exposure to ambient air (below 48 h). The quantitative analysis of the O 1s peaks, however, reveals that the as-grown standard material shows an about 5 times higher O content. This can be understood considering that the presence of Na is known to catalyze the oxidation of In and Ga on chalcopyrite surfaces.[8] In fact, for the as-grown standard CIGSe sample, we find spectral features in the In MNN and Ga LMN Auger spectra, which point to a pronounced oxidation of these elements. In contrast, the data for the as-grown Na-free sample show distinctly less oxidation. Because both as-grown samples do not show any oxidation features of Cu and the KCN etching treatment completely removes the indium and gallium oxides from the surface, the surface concentration ratio [Cu]/([In] + [Ga]) is slightly higher for the standard material (at $T \leq 100$ °C) due to preferential removal of oxidized Ga and In. It is suggested that the consecutive annealing at 170 °C leads to a heat-induced elemental redistribution, which adjusts the surface Cu contents of both samples to the same value of about 0.4 (see also the discussion below).

The corresponding data for the Cu-rich sample result in a similar [Cu]/([In] + [Ga]) value after KCN etching compared to the one for the standard sample. However, annealing temperatures above 170 °C lead to a severe increase in the relative surface Cu content, supporting an increased elemental diffusivity at this temperature. The values adjust close to the corresponding integral value of [Cu]/([In] + [Ga]) = 0.93 at T > 250 °C. As shown in the lower row of Figure 3, the compositional changes in the relative surface Ga content due to annealing are very similar for all three samples and point to a slight increase in the Ga concentration at the surface, where overall the values are reduced compared to the integral value (gray dashed line in Figure 3).

Besides the heat-induced compositional changes, we also evaluated changes in the XPS core-level peak positions due to the UHV heat treatment. Figure 4 displays the variations in the binding energies of the Cu $2p_{3/2}$, In $3d_{5/2}$, Ga $2p_{3/2}$, and Se $3d_{5/2}$ core levels, where the peak positions are normalized to the state prior to any heat treatment. For the standard and Na-free samples, we find a significant gradual increase in the binding energy for all core levels of up to 0.6 eV. The fact that the core levels shift collectively in the binding energy shows that this effect is not related to any changes in the chemical environment of the involved elements. Rather, this collective increase in the binding energy shows that the increasing annealing temperature leads to a pronounced surface downward band bending. In contrast, the Cu-rich sample shows only minor changes in the binding energies of the different peaks.

In a previous study conducted on $CuInSe_2$ surfaces, it was suggested that the presence of Na could be the source of positive surface charge and therefore the reason for the heat-

DOI: 10.1021/acsami.5b03260
ACS Appl. Mater. Interfaces 2015, 7, 13062−13072

induced type inversion after UHV annealing at chalcopyrite surfaces.[30] Therefore, we found it surprising that the Na-free sample shows the same heat-induced increase in surface band bending as the standard sample. Figure 5 shows the XPS

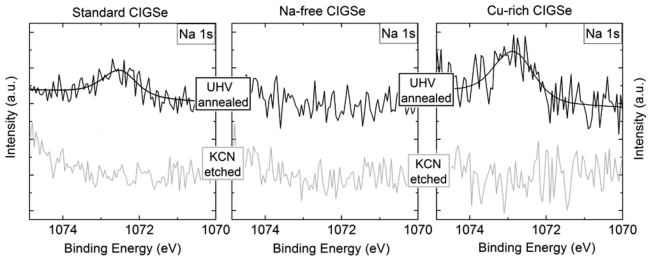

Figure 5. Na 1s core-level spectra after KCN etching and after annealing to 280 °C in UHV. The spectra are normalized to the background at the lower-binding-energy side and subsequently offset for better comparability.

spectra of the Na 1s region for the KCN-etched state and after annealing to 280 °C. After KCN etching, the data clearly show the absence of any Na species at the surface for all samples. However, after the 280 °C UHV heat treatment, we find a small amount of Na in the case of the standard and Cu-rich sample materials, which, thermally activated, diffused to the respective surface. The spectra for the Na-free sample expectedly prove its absence.

For the samples that were heated to 280 °C in a single UHV annealing step (open symbols in Figures 3 and 4), we also performed UPS experiments after KCN etching and after subsequent annealing, where we determined the energetic position of the VBM E^S_{vbm} (spectra shown in Figure S5 in the SI; values summarized in Table 1). Additionally, by measure-

Table 1. Work Function (W), VBM from UPS (E^S_{vbm}), Change in the Band Bending As Determined by XPS Peak Shifts in Figure 4 (ΔBB), and Surface Dipole δ for All Three CIGSe Materials after KCN Etching and a Subsequent Single-Step UHV Annealing at 280°C for 30 min[a]

	$W \pm 0.05$ (eV)	$E^S_{vbm} \pm 0.05$ (eV)	ΔBB ± 0.07 (eV)	$\delta \pm 0.4$ (eV)
		Standard Sample		
KCN	4.81	0.52	:=0	−0.7
UHV-annealed	5.29	0.85	0.43	+0.1
		Na-Free Sample		
KCN	4.60	0.50	:=	−0.9
UHV-annealed	5.18	0.85	0.47	0.0
		Cu-Rich Sample		
KCN	5.14	0.56	:=0	+0.3
UHV-annealed	5.68	0.59	0.17	+0.9

[a]The values for ΔBB are averaged over the different shifts of the XPS peaks (open symbols in Figure 4). Details about the calculation of the surface dipoles are given as SI.

ment of the secondary electron cutoff energy for each sample state, the corresponding work functions W were determined (Table 1). All three samples show an increase in the work function of about half of an electronvolt due to UHV annealing, which counterintuitively goes along with the observed heat-induced downward band bending. As illustrated by a schematic energy-level diagram in Figure 6b, if the change in the work function was due to the band bending alone, one would expect

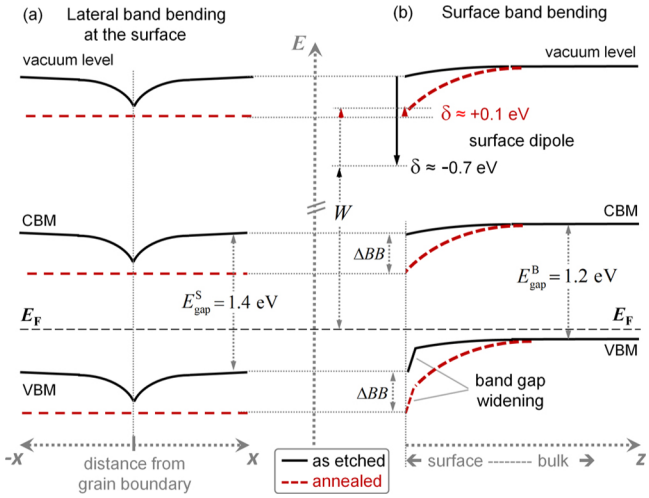

Figure 6. Energy-level diagram illustrating the relationship of lateral band bending effects at grain boundaries (a) and the (vertical) downward band bending at the surface (b) of Cu-poor grown chalcopyrite thin films (the given values correspond to the standard CIGSe sample). The band-gap widening at the surface due to Cu depletion is illustrated as a linear band-gap widening at the VBM. The lateral and vertical band bendings lead to a two-dimensional band diagram at grain boundaries.

a corresponding decrease in the work function. Therefore, the heat treatment must involve a change in the surface dipole δ for all sample materials. To get an idea about the quantitative surface dipoles before and after the heat treatment, we estimated the corresponding values. While the details of the calculations and an error analysis are provided as SI, the results are given in the very right column in Table 1. Note the significant errors for the surface dipoles, which are based on the uncertainties within the estimation. Nevertheless, because of the large changes in the surface dipoles, these findings help to understand the heat-induced processes at the surfaces as discussed below.

DISCUSSION

Grain-Boundary Effects. The lateral defect-level density distribution of the standard and Na-free material as measured by STS shows qualitatively very similar signatures (Figure 2). In particular, before the UHV heat treatment, both samples show a reduced dI/dU contrast at grain boundaries in the vicinity of E_F (U = 0.0 V). Moreover, both samples show a similar downward band bending toward the grain boundaries, which can be seen in the single STS spectra recorded at different distances from various grain boundaries (Figure S2 and S3 in the SI) and particularly well by the gradual characteristics in the dI/dU movies at positive bias voltages. The downward band bending toward grain boundaries is in accordance with previous STS results from both as-grown and KCN-etched standard CIGSe thin films.[12,39] In these studies, it was suggested that both grain-boundary effects (passivation of deep defects and band bending) could be related to the presence of Na. In fact, a possible passivation of grain boundaries involving Na has been discussed in the literature for over a decade.[8,27−29] The data for the standard and Na-free material presented in Figure 2 now allow (supported by our XPS results) to exclude the presence of Na as the origin for these effects.

In the past, there have been numerous investigations of chalcopyrite materials using Kelvin probe force microscopy

DOI: 10.1021/acsami.5b03260
ACS Appl. Mater. Interfaces 2015, 7, 13062−13072

(KPFM), providing access to local work function changes and hence lateral band-bending effects at grain boundaries. Most studies report an increased surface potential of about 100−300 mV, which can be associated with a downward band bending at grain boundaries.[10,11,40] While a rigid quantitative analysis of the lateral grain-boundary band bending from the STS data is difficult, the combined analysis of single spectra and the dI/dU movies allows to estimate that the observed band bending (with and without Na) is in the same range. In a recent KPFM study utilizing a new way of data analysis, however, pronounced fluctuations in the potential changes are reported, implying downward as well as upward band bending,[13] which cannot be confirmed by our results for the standard absorber material with slight Cu deficiency and an integral Ga content of about [Ga]/([In] + [Ga]) = 0.3.

The UHV heat treatment for the standard and Na-free samples leads to a homogeneous passivation of the surfaces without any noticeable grain-boundary effects, implying the absence of lateral potential changes (i.e., lateral band bending) at grain boundaries (see also Figure 6 and the discussion including vertical band bending below).

In the case of the Cu-rich grown material prior to UHV annealing, most of the surface area is already passivated without any significant grain-boundary effects. This suggests that the grain-boundary effects observed for the standard and Na-free material prior to the heat treatment must be related to Cu deficiency. Under Cu-poor conditions, Cu vacancies (V_{Cu}) and (In,Ga)-on-Cu antisite defects [$(In,Ga)_{Cu}$] are the most prominent defects in the bulk as well as on surfaces and grain boundaries.[6,7,41] Therefore, these defects should be considered to play a dominant role for the observed grain-boundary passivation and lateral band-bending effects.

Surface Cu Depletion and Type Inversion. The pronounced collective XPS peak shifts to higher binding energies observed for both the standard and Na-free samples point to an accumulation of positive surface charge and a related increasing surface downward band bending induced by the UHV annealing. As previously shown for $CuInSe_2$, such a strong band bending ultimately leads to type inversion at the surface. It was suggested that the positive surface charge could be related to the presence of small amounts of Na, which heat-induced diffuse to the surface.[30,42,43] However, our data for the Na-free sample show the same pronounced surface downward band bending after the heat treatment as the standard sample. Because we evidently do not observe any Na on the surface after the annealing of this sample (Figure 5, center), Na can, hence, be safely excluded as the origin for this effect. Note that for none of the investigated samples we did observe the presence of K at the surface.

As discussed above, the observed increasing surface band bending for the standard and Na-free materials due to the heat treatment goes along with changes of the lateral band bending at grain boundaries (from downward band bending to flat bands). Thereby, the combination of surface band bending and lateral band bending at spatially extended grain boundaries results in a complex three-dimensional alignment of the energy levels. To visualize this, parts a and b of Figure 6 sketch both in a comparative way, the lateral band bending at grain boundaries, which is shown for the case at the surface (part a), and the band bending from the bulk toward the surface (surface band bending; part b). Because of the UHV annealing, the surface band bending increases from nearly flat-band conditions by several hundred millielectronvolts, leading to type inversion (indicated by the red dashed line in Figure 6b). In the STS experiments after the etching procedure, we observe a distinct downward band bending toward most of the grain boundaries. The UHV annealing, in turn, levels these electronic inhomogeneities out, leading to a uniform potential distribution at the surface, as indicated by the red dashed line in Figure 6a. This means that close to the grain boundaries the heat-induced change in the surface band bending ΔBB is significantly smaller than that on the grain centers. This, in turn, suggests that, prior to the UHV heat treatment, the energy levels at the grain boundaries are pinned downward with respect to the grain centers. Therefore, after the annealing, an equally strong surface downward band bending on the grains and grain boundaries is obtained. Note, however, that this does not exclude a possible lateral grain-boundary band bending within the bulk of the absorber. Rather, the pronounced photocurrents at grain boundaries measured by conductive atomic force microscopy[34] suggest that there still could be a pronounced grain-boundary band bending in the bulk.[34] This would imply when one moves from the surface (with a homogeneous potential distribution) toward the bulk, the surface-induced space charge decreases, while the grain-boundary space charge might still be intact.

In contrast to the standard and Na-free samples, the Cu-rich grown material shows only a weak change in the surface band alignment upon the UHV annealing (Figure 4, right). Therefore, no surface charge is built up because of the heat treatment in this case. Given the widely passivated state of the Cu-rich sample after KCN etching as well as after the heat treatment, the surface defect physics of the Cu-rich material must significantly differ from the Cu-poor grown material. This again suggests that, under Cu-poor conditions, V_{Cu} and/or (In,Ga)-on-Cu antisite defects play a crucial role in surface type inversion.[7,18] In fact, the correlation of surface type inversion and Cu depletion on surfaces of chalcopyrite films with a substoichiometric integral Cu content must be closely related to these findings.[15,19] Therefore, the present results must be discussed in view of the controversial debate about the origin of Cu depletion and the related type inversion at chalcopyrite thin-film surfaces. The most discussed model assumes a bulklike ordered defect compound (ODC) phase with n-type conductivity, segregating at the surface of chalcopyrite films grown under slightly Cu-poor conditions.[15,18] This model is based on the findings from first-principles calculations predicting the favorable formation of ordered defect pairs, where two negatively charged Cu vacancies ($2V_{Cu}^{-}$) and an In_{Cu}^{2+} defect form a charge-compensated $(2V_{Cu}^{-} + In_{Cu}^{2+})^{0}$ complex.[18] However, this model applied to an ODC layer segregated at the surface is lacking experimental evidence,[20,23,33,44] and very recent results from screened-exchange hybrid density functional theory cast doubt on the findings about the mechanisms, leading to an energetically favorable formation energy of such an ODC phase.[7]

A different model, which combines the Cu depletion and type inversion for chalcopyrite surfaces, is proposed by Herberholz et al.[19] The authors suggest that positive charges at the surface induce a vertical downward band bending. According to the model, the electric field of the related space charge leads to the electromigration of mobile Cu^{+} ions into the bulk of the material, depleting the surface of Cu. This model is supported by low activation barriers for Cu diffusion via interstitial sites, as determined from ab initio simulations.[21] From this point of view, the surface Cu content should significantly correlate with the heat-induced surface downward

DOI: 10.1021/acsami.5b03260
ACS Appl. Mater. Interfaces 2015, 7, 13062−13072

band bending observed for the standard and Na-free samples in our experiments. However, the XPS data for both samples show only a minor reduction in the surface Cu content, which hardly correlates with the increasing surface band bending (Figures 3 and 4). While, in principle, this could still indicate a slight electromigration of Cu ions into the bulk in the case of the standard sample, the Na-free material shows a similar band bending with an even lower reduction in the surface Cu content. As discussed above, in the case of the standard sample, the reduction in the surface Cu content is attributed to a stronger preferential oxidation of In and Ga as catalyzed by the presence of Na. After removal of the oxides by the KCN etching, the surface appears less Cu-depleted compared to the Na-free sample, where subsequent elemental redistribution induced by the UHV annealing at $T \geq 170$ °C adjusts the surface Cu content to similar values for the two samples. From these considerations, it appears that the electromigration of Cu^+ ions is not a dominating effect in the mechanism, leading to Cu depletion of chalcopyrite thin-film surfaces.

In the past few years, several experimental studies on epitaxial and polycrystalline chalcopyrite films revealed that instead of a surface layer extending significantly into the bulk of the material, the Cu depletion is limited to only the top few atomic layers, which are extremely depleted of Cu atoms.[23,24,45] These findings are in agreement with ab initio calculations, taking the lattice symmetry breaking of the surface into account. This allowed to explain the unusual stability of polar chalcopyrite surfaces as well as the surface Cu depletion by a defect-induced surface reconstruction for Cu-poor integral compositions. According to this model, the surface dipoles are compensated by the presence of Cu vacancies or (In,Ga)-on-Cu antisite defects at the surface (depending on the individual facet termination). Because of the extremely low formation energies for these defects, the polar facets are favored over the nonpolar ones. Because the defect formation energies in this reconstruction depend on the overall Cu content of the material, under Cu-rich conditions, different defects and, as a consequence, different surface facets are favored.[6,22] The different surface defects are probably the reason why the surface is not able to stabilize positive charge, which could lead to a band bending under Cu-rich conditions. In contrast, in the case of the Cu-poor samples, Cu vacancies, (In,Ga)-on-Cu antisite defects, or related defect combinations are the most likely candidates to carry the positive surface charge (similar to the above-discussed grain-boundary band bending), which induces the strong surface band bending in this case. However, here it should be noted that in ab initio calculations usually a zero net charge within the corresponding slab models is assumed. Therefore, this approach does not take into account the possibility of trapped charges, which could induce a space charge. Nevertheless, the total amount of charge to induce a band bending in a semiconductor is usually below 0.1% of the surface atoms, which probably has no significant effect on the reconstruction mechanism itself.

One of the experimental studies that support the surface reconstruction model mentioned above involved an analysis by synchrotron-excited HAX-PES. With this experimental technique, depth-dependent compositional information can be obtained by varying the escape depth of the probed photoelectrons by controlling the excitation energy by several kiloelectronvolts. As previously reported, the results for standard Cu-poor grown CIGSe samples after removal of surface oxides by KCN etching suggest that the Cu depletion is restricted to an extremely thin surface layer, which is completely depleted of Cu atoms.[24,46] However, the CIGSe surface after oxide removal by the KCN treatment is not type-inverted and, hence, does not allow to directly correlate the Cu depletion with the type inversion at the surface. Furthermore, as discussed above, the surface Cu content depends slightly on the degree of preferential In and Ga oxidation. Therefore, we performed an additional HAX-PES experiment to elucidate to what extent the UHV heat treatment affects the depth-dependent Cu concentration of a standard CIGSe material. Figure 7 shows the relative corrected photoelectron intensity

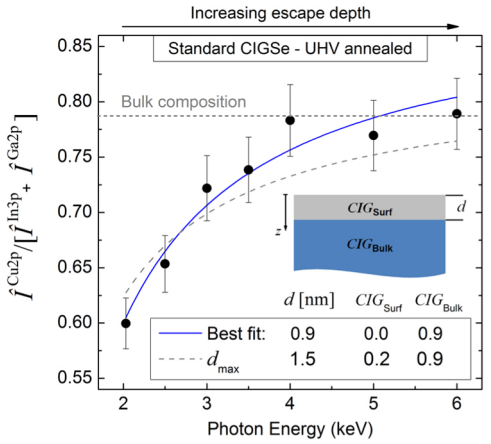

Figure 7. Relative corrected core-level intensities for Cu $2p_{3/2}$, In $3p_{3/2}$, and Ga $2p_{3/2}$ measured by HAX-PES as a function of the photon energy for the standard CIGSe material after KCN etching and subsequent UHV annealing at 280 °C for 30 min. The increasing photon energy results in an increasing escape depth and a related increasing information depth. The data are fitted to a bilayer model depicted as an inset. For the fitting, the relative Cu content CIG = [Cu]/([In] + [Ga]) in the bulk CIG_{Bulk}, in the surface layer CIG_{Surf}, and the thickness of the surface layer d were varied. The blue solid line shows the optimum fit. To check the accuracy for the surface layer thickness, we find an upper limit with about d = 1.5 nm (gray dashed line). Details about this approach have been reported previously.[24]

$\hat{I}^{Cu\ 2p}/(\hat{I}^{In\ 3p} + \hat{I}^{Ga\ 2p})$ as a function of the photon energy for the standard CIGSe sample after KCN etching and subsequent UHV annealing. The UHV annealing leads to a slightly more pronounced increase of the relative corrected intensity compared to the previously reported data for a similar sample directly after KCN etching.[24] Nevertheless, as suggested by the fits in Figure 7, the surface is still extremely Cu-depleted in a very thin surface layer, which extends only a few atomic layers into the bulk. Therefore, we are able to experimentally correlate this Cu depletion with a type inversion at the surface, providing strong evidence for a defect-induced surface reconstruction as its origin. A thermally activated formation of an extended (bulklike) Cu-depleted defect phase at the surface can be excluded. Therefore, the VB offset and related band-gap widening at the CIGSe/CdS interface due to are Cu depletion (see Figure 1b) is restricted to only a few atomic layers. This, in turn, implies increased thermionic excitation of photoexcited holes by tunneling and thus increased recombination losses at the CIGSe/CdS interface. The situation becomes more complex when the presence of K is taken into account. The recently achieved efficiency gains due to the KF postdeposition treatment were shown to go along with a pronounced extrusion of Cu atoms from the chalcopyrite matrix at the surface/

DOI: 10.1021/acsami.5b03260
ACS Appl. Mater. Interfaces 2015, 7, 13062−13072

interface.[1] On top of this, this effect might vary with the Ga content.[47] Therefore, on the basis of the current state of research, the K-driven Cu depletion should be discussed independently from the intrinsic surface Cu depletion discussed here.

Surface Passivation and Dipole Effects. As observed in our UHV annealing experiments for the Cu-poor grown samples, the surfaces do not only invert electronically because of the heat treatment, but also our STS data show that this type inversion goes along with a passivation of the surface defect levels. Because this heat-induced passivation is also found for the Na-free sample, the presence of Na can also be excluded as a major factor leading to this effect. Furthermore, taking our previous work from $CuInSe_2$ into account, the Ga content of $[Ga]/([In] + [Ga]) \approx 0.3$ in our samples also does not have a significant effect on this passivation mechanism either. As found by the estimation of the surface dipole for the sample states directly after KCN etching and after UHV annealing (Table 1), again the standard and Na-free samples (both Cu-poor grown) show very similar behavior. After KCN etching, the standard and Na-free samples show a similar negative surface dipole of $\delta = -0.7$ and -0.9 eV, respectively. Most interestingly, in both cases, the heat treatment leads to a pronounced reduction of the dipoles close to zero. This suggests that the removal of surface oxides (mainly indium and gallium oxides) by KCN etching leads to broken bonds, which result not only in a high density of defect levels, as observed in our STS data, but also in a negative surface dipole. The UHV annealing, in turn, reorganizes the distribution of the elements saturating the broken bonds, which eliminates the defect levels and compensates the initial negative dipole at the surface. Note that this is supported by an estimation of the indium or gallium oxide coverage at the surface, revealing three monolayers for the standard material and about one monolayer for the Na-free material.

The theoretical work by Hinuma et al. proposes a surface reconstruction model, which stabilizes polar facets and at the same time does not lead to localized defect levels in $CuInSe_2$ or $CuGaSe_2$ under Cu-poor conditions.[6] In line with our experiments, these results indicate the possibility of an intrinsic passivation of chalcopyrite surfaces without the necessity of the presence of impurities like alkali metals, O, or elements from the buffer layer. Moreover, this work explains the absence of a significant surface dipole, which is in agreement with our data from the Cu-poor grown samples after the heat treatment and the associated elemental redistribution at the surface.

In contrast to the Cu-poor grown samples, the STS data of the Cu-rich sample show a passivated state of the surface before and after the heat treatment with a reduced surface band gap (Figure 2). The reduced surface band gap is also in agreement with the surface reconstruction model, which, for Cu-rich compositions, predicts electronic states at the VB edge, lowering the surface band gap by about 0.2 eV compared to the Cu-poor case.[6] Before the heat treatment, we observe a positive surface dipole with $\delta = 0.3$ eV, which, regarding the large error, indicates only a minor dipole in this case. The absence of a significant defect density in the energy range of the band gap before the heat treatment of the Cu-rich grown sample opposes our findings for the Cu-poor samples, which show a high defect density prior to the UHV annealing. This shows that, under Cu-rich conditions, different defect chemical mechanisms at the surface are favored, which is in line with our discussion about the absence of a significant heat-induced band bending (see above). This is further supported by the significant positive surface dipole ($\delta = +0.9$ eV) after the UHV annealing. The change of the surface dipole in this case is probably related to the severe heat-induced increase in the surface Cu content, which adjusts close to the integral Cu content (Figure 3, right). The positive sign of the dipole in the case of the Cu-rich sample suggests an anion termination and thus a preferential $(\overline{1}12)$ surface faceting without any dipole-compensating defects. This is in accordance with additional XPS experiments after air annealing (200 °C, 30 min), where we found a distinct selenium oxidation only for the Cu-rich sample, whereas the Cu-poor samples do not show any oxidation features for the chalcogen (see Figure S7 in the SI). None of the samples showed spectral signatures pointing to any Cu oxidation after this heat treatment in air. The presence of selenium oxide after air annealing exclusively on the Cu-rich sample indicates that indeed in this case the surface could be dominated by polar facets with Se termination. Here it should be emphasized that the different surface termination for Cu-poor and -rich grown material is also reflected in the different surface morphologies.[24,48]

CONCLUSIONS

The surfaces of standard and Na-free CIGSe samples show very similar defect chemical characteristics and electronic properties. Prior to the UHV heat treatment, the materials both with and without a Na diffusion barrier show a high defect-level density on most of the grains, a reduced density of deep-level defects, and similar lateral downward band bending at grain boundaries, excluding the presence of residual amounts of Na as a decisive parameter for these grain-boundary effects. A UHV heat treatment induces the diffusion of submonolayer amounts of Na accumulating only at the surface of the standard sample. However, the defect levels at the surface of both standard and Na-free CIGSe are completely passivated because of the heat treatment. Furthermore, both materials exhibit the same heat-induced surface downward band bending of up to 600 meV, leading to surface type inversion. Taking the pronounced lateral grain-boundary band bending prior the heat treatment into account allows to conclude that the heat-induced change in the surface band bending ΔBB is strongest on the grain centers, gradually decreasing with the degree of (lateral) band bending toward the grain boundaries, leading to a homogeneous lateral potential distribution and a surface dipole compensation, as depicted in Figure 6.

In contrast to the presence of Na, the integral Cu content does significantly affect the defect chemical properties of chalcopyrite surfaces. Terminating the coevaporation process within the Cu-rich phase leads to the well-known copper selenide segregation at the surface. After wet chemical removal of these secondary phases, the surface appears widely passivated without any significant grain-boundary effects. Small regions covering about 5−10% of the surface area with high conductance at positive bias voltages are observed, implying high densities of unoccupied (donor-type) defects. After the heat treatment in UHV, these areas are passivated as the rest of the surface. However, unlike the Cu-poor material, Cu-rich grown samples show hardly any change in the surface band bending due to the heat treatment and the Fermi level stays around midgap. The different defect chemistry and resulting different electronic surface properties of the Cu-rich CIGSe material are attributed to the absence of Cu vacancies or (In,Ga)-on-Cu antisite defects at the surface of the Cu-rich

DOI: 10.1021/acsami.5b03260
ACS Appl. Mater. Interfaces 2015, 7, 13062−13072

material. Its different surface defect chemistry compared to standard CIGSe is also reflected in the different oxidation behavior and surface morphology. This suggests that, under Cu-rich growth conditions, different surface facet orientations or terminations are favored.

Our results provide evidence that the type inversion at the surface of standard (Cu-poor grown) chalcopyrite materials is dominated by band bending accompanied by a widening of the surface band gap, rather than due to the segregation of a bulklike defect compound with n-type conductivity at the surface. As we also find no significant correlation of the surface Cu content and degree of vertical surface band bending in the standard material, a surface Cu depletion driven by electromigration of Cu ions in the surface field seems unlikely. In contrast, our experiments by synchrotron-excited HAX-PES confirm that the n-type conductivity goes along with an extreme surface Cu depletion, which is restricted to the top atomic layers. This supports a theoretical model that explains the surface Cu depletion of standard chalcopyrite materials by a defect-induced surface reconstruction, where only atoms in the first few layers are subject to compositional and electronic reorganization with respect to the bulk.

METHODS

Scanning Tunneling Microscopy (STM)/STS. The STS investigations were conducted in a commercial scanning tunneling microscope (STM) from Omicron Nanotechnology (VT-AFM/STM) at room temperature and at a base pressure in the 10^{-10} mbar range. For the tips, we used electrochemically etched tungsten wires. Locally resolved $I(U)$ spectra were recorded by sweeping the bias voltage in a range between −2.3 and +2.0 V while the feedback loop was disabled. Spectra were recorded every 10 nm on large equally spaced grids, which leads to extensive acquisition times of about 12−36 h (depending on the image size) for complete data sets. After numerical differentiation of the $I(U)$ spectra, the resulting three-dimensional data set $[x, y, \mathrm{d}I/\mathrm{d}U(U)]$ was then converted to obtain (x, y) plots of the differential conductivity $\mathrm{d}I/\mathrm{d}U$ as a function of U, which are interpreted in terms of the lateral defect density distribution at energies eU. For the recording of the $I(U)$ spectra, we set a current limit at 5 nA. In Figure 2, sites where this current limit is exceeded are marked in blue. All bias voltages are given with respect to the sample, where negative/positive voltages correspond to probing occupied/unoccupied states, respectively.

XPS/UPS. Photoelectron spectroscopy experiments with laboratory sources were performed in a commercial UHV system from SPECS, which is equipped with a PHOIBOS 100 hemispherical analyzer and a delayline detector. For excitation, we used a monochromated Al Kα X-ray source and HeI/HeII UV radiation. For experiments to determine the work function by measuring the secondary electron cutoff, a bias voltage of 5.00 V was applied to the sample, shifting the spectrum to lower binding energies. All XPS/UPS data were recorded in normal emission at room temperature and at a base pressure in the 10^{-10} mbar range.

HAX-PES. Hard X-ray photoelectron spectroscopy was conducted with the HIKE end station at the KMC-1 beamline at the BESSY synchrotron facility in Berlin. The experiments were performed under UHV conditions in the low 10^{-9} mbar range with an R-4000 hemispherical electron analyzer from Scienta optimized for high kinetic electron energies. Further experimental details can be found elsewhere.[24]

Sample Growth. Details about the growth of the investigated chalcopyrite thin films are already given at the beginning of the Results section. Integral compositions were determined by X-ray fluorescence. Reference solar cells with a device structure Mo/CIGSe/CdS/i-ZnO/ZnO:Al were fabricated for the three sample materials. The resulting mean efficiencies are standard 15.5% (maximum: 16.3%), Na-free 9.1% (maximum: 12.1%), and Cu-rich (CdS deposition after KCN etching to remove Cu_xSe phases) 4.1% (maximum: 7.1%). After growth, the CIGSe samples were stored under an inert gas atmosphere. The total exposure to ambient air was comparable for all samples and below 48 h. In none of the investigated sample states we observed a spectral signature indicating the presence of K.

ASSOCIATED CONTENT

Supporting Information

SEM images of the Cu-rich sample, band-bending effects at grain boundaries, XPS/UPS VB spectra, surface dipole calculations, Se 3d spectra after air annealing, and six individual movies of the data in Figure 2; dIdU CITS Standard CIGSe KCN-etched (file 002), dIdU CITS Standard CIGSe UHV-annealed (file 003), dIdU CITS Na-free CIGSe KCN-etched (file 004), dIdU CITS Na-free CIGSe UHV-annealed (file 005), dIdU CITS Cu-rich CIGSe KCN-etched (file 006), and dIdU CITS Cu-rich CIGSe UHV-annealed (file 007). The Supporting Information is available free of charge on the ACS Publications website at DOI: 10.1021/acsami.5b03260.

AUTHOR INFORMATION

Corresponding Author

*E-mail: harry.moenig@uni-muenster.de.

Author Contributions

§These authors contributed equally to this work.

Notes

The authors declare no competing financial interest.

ACKNOWLEDGMENTS

The authors acknowledge technical support by the BESSY staff (especially M. Gorgoi). We thank J. Sondhauß for support in acquiring the SEM images presented as SI.

REFERENCES

(1) Chirila, A.; Reinhard, P.; Pianezzi, F.; Bloesch, P.; Uhl, A. R.; Fella, C.; Kranz, L.; Keller, D.; Gretener, C.; Hagendorfer, H.; Jaeger, D.; Erni, R.; Nishiwaki, S.; Buecheler, S.; Tiwari, A. N. Potassium-Induced Surface Modification of $Cu(In,Ga)Se_2$ Thin Films for High-Efficiency Solar Cells. *Nat. Mater.* **2013**, *12*, 1107−1111.

(2) Jackson, P.; Hariskos, D.; Wuerz, R.; Wischmann, W.; Powalla, M. Compositional Investigation of Potassium Doped $Cu(In,Ga)Se_2$ Solar Cells with Efficiencies up to 20.8%. *Phys. Status Solidi RRL* **2014**, *8*, 219−222.

(3) Jackson, P.; Hariskos, D.; Wuerz, R.; Kiowski, O.; Bauer, A.; Friedlmeier, T. M.; Powalla, M. Properties of $Cu(In,Ga)Se_2$ Solar Cells with New Record Efficiencies up to 21.7%. *Phys. Status Solidi RRL* **2015**, *9*, 28−31.

(4) Siebentritt, S. What Limits the Efficiency of Chalcopyrite Solar Cells? *Prog. Photovoltaics* **2011**, *95*, 1471−1476.

(5) Zhang, S. B.; Wei, S. H.; Zunger, A.; Katayama-Yoshida, H. Defect Physics of the $CuInSe_2$ Chalcopyrite Semiconductor. *Phys. Rev. B* **1998**, *57*, 9642−9656.

(6) Hinuma, Y.; Oba, F.; Kumagai, Y.; Tanaka, I. Ionization Potentials of (112) and $(11\bar{2})$ Facet Surfaces of $CuInSe_2$ and $CuGaSe_2$. *Phys. Rev. B* **2012**, *86*, 245433-1−245433-7.

(7) Pohl, J.; Albe, K. Intrinsic Point Defects in $CuInSe_2$ and $CuGaSe_2$ as Seen via Screened-Exchange Hybrid Density Functional Theory. *Phys. Rev. B* **2013**, *87*, 245203-1−245203-16.

(8) Kronik, L.; Cahen, D.; Schock, H.-W. Effects of Sodium on Polycrystalline $Cu(In,Ga)Se_2$ and its Solar Cell Performance. *Adv. Mater.* **1998**, *10*, 31−36.

(9) Jiang, C.-S.; Noufi, R.; Ramanathan, K.; Moutinho, H. R.; Al-Jassim, M. M. Electrical Modification in $Cu(In,Ga)Se_2$ Thin Films by Chemical Bath Deposition Process of CdS Films. *J. Appl. Phys.* **2005**, *97*, 053701-1−053701-6.

DOI: 10.1021/acsami.5b03260
ACS Appl. Mater. Interfaces 2015, 7, 13062−13072

(10) Yan, Y.; Jiang, C.-S.; Noufi, R.; Wei, S.-H.; Moutinho, H. R.; Al-Jassim, M. M. Electrically Benign Behavior of Grain Boundaries in Polycrystalline $CuInSe_2$ Films. *Phys. Rev. Lett.* **2007**, *99*, 235504-1−235504-4.
(11) Rau, U.; Taretto, K.; Siebentritt, S. Grain Boundaries in $Cu(In,Ga)Se_2$ Thin-Film Solar Cells. *Appl. Phys. A: Mater. Sci. Process.* **2009**, *96*, 221−234.
(12) Mönig, H.; Smith, Y.; Caballero, R.; Kaufmann, C. A.; Lauermann, I.; Lux-Steiner, M. C.; Sadewasser, S. Direct Evidence for a Reduced Density of Deep Level Defects at Grain Boundaries of $Cu(In,Ga)Se_2$ Thin Films. *Phys. Rev. Lett.* **2010**, *105*, 116802-1−116802-4.
(13) Baier, R.; Leendertz, C.; Abou-Ras, D.; Lux-Steiner, M. C.; Sadewasser, S. Properties of Electronic Potential Barriers at Grain Boundaries in $Cu(In,Ga)Se_2$ Thin Films. *Sol. Energy Mater. Sol. Cells* **2014**, *130*, 124−131.
(14) Yin, W.-J.; Wu, Y.; Noufi, R.; Al-Jassim, M.; Yan, Y. Defect Segregation at Grain Boundary and its Impact on Photovoltaic Performance of $CuInSe_2$. *Appl. Phys. Lett.* **2013**, *102*, 193905−1−4.
(15) Schmid, D.; Ruckh, M.; Grunewald, F.; Schock, H. W. Chalcopyrite Defect Chalcopyrite Heterojunctions on the Basis of $CuInSe_2$. *J. Appl. Phys.* **1993**, *73*, 2902−2909.
(16) Morkel, M.; Weinhardt, L.; Lohmüller, B.; Heske, C.; Umbach, E.; Riedl, W.; Zweigart, S.; Karg, F. Flat Conduction-Band Alignment at the $CdS/CuInSe_2$ Thin-Film Solar-Cell Heterojunction. *Appl. Phys. Lett.* **2001**, *79*, 4482−4484.
(17) Bär, M.; Repins, I.; Contreras, M. A.; Weinhardt, L.; Noufi, R.; Heske, C. Chemical and Electronic Surface Structure of 20%-Efficient $Cu(In,Ga)Se_2$ Thin Film Solar Cell Absorbers. *Appl. Phys. Lett.* **2009**, *95*, 052106-1−052106-3.
(18) Zhang, S. B.; Wei, S. H.; Zunger, A. Stabilization of Ternary Compounds via Ordered Arrays of Defect Pairs. *Phys. Rev. Lett.* **1997**, *78*, 4059−4062.
(19) Herberholz, R.; Rau, U.; Schock, H. W.; Haalboom, T.; Gödecke, T.; Ernst, F.; Beilharz, C.; Benz, K. W.; Cahen, D. Phase Segregation, Cu Migration and Junction Formation in $Cu(In,Ga)Se_2$. *Eur. Phys. J.: Appl. Phys.* **1999**, *6*, 131−139.
(20) Rau, U.; Schock, H. W. Electronic Properties of $Cu(In,Ga)Se_2$ Heterojunction Solar Cells—Recent Achievements, Current Understanding, and Future Challenges. *Appl. Phys. A: Mater. Sci. Process.* **1999**, *69*, 131−147.
(21) Pohl, J.; Klein, A.; Albe, K. Role of Copper Interstitials in $CuInSe_2$: First-Principles Calculations. *Phys. Rev. B* **2011**, *84*, 121201-1−121201-4.
(22) Jaffe, J. E.; Zunger, A. Defect-Induced Nonpolar-to-Polar Transition at the Surface of Chalcopyrite Semiconductors. *Phys. Rev. B* **2001**, *64*, 241304-1−241304-4.
(23) Liao, D. X.; Rockett, A. Cu Depletion at the $CuInSe_2$ Surface. *Appl. Phys. Lett.* **2003**, *82*, 2829−2831.
(24) Mönig, H.; Fischer, C. H.; Caballero, R.; Kaufmann, C. A.; Allsop, N.; Gorgoi, M.; Klenk, R.; Schock, H.-W.; Lehmann, S.; Lux-Steiner, M. C.; Lauermann, I. Surface Cu Depletion of $Cu(In,Ga)Se_2$ Films: An Investigation by Hard X-ray Photoelectron Spectroscopy. *Acta Mater.* **2009**, *57*, 3645−3651.
(25) Klenk, R.; Lux-Steiner, M. C. In *Thin Film Solar Cells: Fabrication, Characterization and Applications*; Poortmans, J., Arkhipov, V., Eds.; John Wiley & Sons Ltd.: New York, 2006; pp 237−266.
(26) Liao, D.; Rockett, A. Cd Doping at the $CuInSe_2/CdS$ Heterojunction. *J. Appl. Phys.* **2003**, *93*, 9380-1−9380-3.
(27) Rudmann, D.; da Cunha, A. F.; Kaelin, M.; Kurdesau, F.; Zogg, H.; Tiwari, A. N.; Bilger, G. Efficiency Enhancement of $Cu(In,Ga)Se_2$ Solar Cells due to Post-Deposition Na Incorporation. *Appl. Phys. Lett.* **2004**, *84*, 1129−1131.
(28) Rockett, A. The Effect of Na in Polycrystalline and Epitaxial Single-Crystal $CuIn_{1-x}Ga_xSe_2$. *Thin Solid Films* **2005**, *480−481*, 2−7.
(29) Laemmle, A.; Wuerz, R.; Schwarz, T.; Cojocaru-Mirédin, O.; Choi, P.-P.; Powalla, M. Investigation of the Diffusion Behavior of Sodium in $Cu(In,Ga)Se_2$ Layers. *J. Appl. Phys.* **2014**, *115*, 154501-1−154501-8.
(30) Mönig, H.; Lockhorn, D.; Aghdassi, N.; Timmer, A.; Kaufmann, C. A.; Caballero, R.; Zacharias, H.; Fuchs, H. Heat Induced Passivation of $CuInSe_2$ Surfaces: A Strategy to Optimize the Efficiency of Chalcopyrite Thin Film Solar Cells? *Adv. Mater. Interfaces* **2014**, *1*, 1300040-1−1300040-7.
(31) Cadel, E.; Barreau, N.; Kessler, J.; Pareige, P. Atom Probe Study of Sodium Distribution in Polycrystalline $Cu(In,Ga)Se_2$ Thin Film. *Acta Mater.* **2010**, *58*, 2634−2637.
(32) Cojocaru-Mirédin, O.; Choi, P.; Wuerz, R.; Raabe, D. Exploring the p−n Junction Region in $Cu(In,Ga)Se_2$ Thin-Film Solar Cells at the Nanometer-Scale. *Appl. Phys. Lett.* **2012**, *101*, 181603-1−181603-5.
(33) Mönig, H.; Fischer, C. H.; Grimm, A.; Johnson, B.; Kaufmann, C. A.; Caballero, R.; Lauermann, I.; Lux-Steiner, M. C. Surface Cu-Depletion of $Cu(In,Ga)Se_2$ Thin Films: Further Experimental Evidence for a Defect-Induced Surface Reconstruction. *J. Appl. Phys.* **2010**, *107*, 113540-1−113540-5.
(34) Azulay, D.; Balberg, I.; Millo, O. Microscopic Evidence for the Modification of the Electronic Structure at Grain Boundaries of of $Cu(In_{1-x},Ga_x)Se_2$ Films. *Phys. Rev. Lett.* **2012**, *108*, 076603-1−076603-4.
(35) Caballero, R.; Kaufmann, C. A.; Efimova, V.; Rissom, T.; Hoffmann, V.; Schock, H. W. Investigation of $Cu(In,Ga)Se_2$ Thin-Film Formation During the Multi-Stage Co-Evaporation Process. *Prog. Photovoltaics* **2013**, *21*, 30−46.
(36) Klenk, R.; Walter, T.; Schock, H.-W.; Cahen, D. A Model for the Successful Growth of Polycrystalline Films of $CuInSe_2$ by Multisource Physical Vacuum Evaporation. *Adv. Mater.* **1993**, *5*, 114−119.
(37) Lehmann, J.; Lehmann, S.; Lauermann, I.; Rissom, T.; Kaufmann, C. A.; Lux-Steiner, M. C.; Bär, M.; Sadewasser, S. Reliable Wet-Chemical Cleaning of Natively Oxidized High-Efficiency $Cu(In,Ga)Se_2$ Thin-Film Solar Cell Absorbers. *J. Appl. Phys.* **2014**, *116*, 233502-1−233502-11.
(38) Regesch, D.; Gutay, L.; Larsen, J. K.; Depredurand, V.; Tanaka, D.; Aida, Y.; Siebentritt, S. Degradation and Passivation of $CuInSe_2$. *Appl. Phys. Lett.* **2012**, *101*, 112108-1−112108-4.
(39) Mönig, H.; Caballero, R.; Kaufmann, C. A.; Schmidt, T. L.; Lux-Steiner, M. C.; Sadewasser, S. Nanoscale Investigations of the Electronic Surface Properties of $Cu(In,Ga)Se_2$ Thin Films by Scanning Tunneling Spectroscopy. *Sol. Energy Mater. Sol. Cells* **2011**, *95*, 1537−1543.
(40) Sadewasser, S.; Glatzel, T.; Schuler, S.; Nishiwaki, S.; Kaigawa, R.; Lux-Steiner, M. Kelvin Probe Force Microscopy for the Nano Scale Characterization of Chalcopyrite Solar Cell Materials and Devices. *Thin Solid Films* **2003**, *431 - 432*, 257−261.
(41) Persson, C.; Zunger, A. Anomalous Grain Boundary Physics in Polycrystalline $CuInSe_2$: The Existence of a Hole Barrier. *Phys. Rev. Lett.* **2003**, *91*, 266401−1−4.
(42) Heske, C.; Fink, R.; Umbach, E.; Riedl, W.; Karg, F. Na-Induced Effects on the Electronic Structure and Composition of $Cu(In,Ga)Se_2$ Thin-Film Surfaces. *Appl. Phys. Lett.* **1996**, *68*, 3431−3433.
(43) Klein, A.; Loher, T.; Pettenkofer, C.; Jaegermann, W. Chemical Interaction of Na with Cleaved (011) Surfaces of $CuInSe_2$. *J. Appl. Phys.* **1996**, *80*, 5039−5043.
(44) Yan, Y.; Jones, K. M.; Abushama, J.; Young, M.; Asher, S.; Al-Jassim, M. M.; Noufi, R. Microstructure of Surface Layers in $Cu(In,Ga)Se_2$ Thin Films. *Appl. Phys. Lett.* **2002**, *81*, 1008−1010.
(45) Cojocaru-Mirédin, O.; Choi, P.; Wuerz, R.; Raabe, D. Atomic-Scale Characterization of the $CdS/CuInSe_2$ Interface in Thin-Film Solar Cells. *Appl. Phys. Lett.* **2011**, *98*, 103504-1−103504-3.
(46) Schorr, S.; Mainz, R.; Mönig, H.; Lauermann, I.; Bär, M. The Complex Material Properties of Chalcopyrite and Kesterite Thin-Film Solar Cell Absorbers Tackled by Synchrotron-Based Analytics. *Prog. Photovoltaics* **2012**, *20*, 557−567.
(47) Ishizuka, S.; Yamada, A.; Fons, P. J.; Shibata, H.; Niki, S. Interfacial Alkali Diffusion Control in Chalcopyrite Thin-Film Solar Cells. *ACS Appl. Mater. Interfaces* **2014**, *6*, 14123−14130.
(48) Liao, D.; Rockett, A. Epitaxial Growth of $Cu(In,Ga)Se_2$ on GaAs(110). *J. Appl. Phys.* **2002**, *91*, 1978−1983.

DOI: 10.1021/acsami.5b03260
ACS Appl. Mater. Interfaces 2015, 7, 13062−13072